

Mathematical modelling of a potential tsunami associated with a late glacial submarine landslide in the Sea of Marmara

Mehmet Sinan Özeren · M. Namık Çağatay ·
Nazmi Postacıoğlu · A. M. Celal Şengör · Naci Görür ·
Kadir Eriş

Received: 14 June 2009 / Accepted: 21 January 2010 / Published online: 20 February 2010
© Springer-Verlag 2010

Abstract Potential tsunami waves were modelled on the basis of the morphology and geological setting of a late glacial submarine landslide localized in the north-eastern sector of the Sea of Marmara, using a three-dimensional algorithm with the purpose of assessing the future risk of tsunamogenic landslides in the region. The landslide occurred off the Tuzla Peninsula on the north-eastern slope of the Çınarcık Basin, the easternmost of the three deep Marmara basins. The mass movement appears to be related to the Main Marmara Fault that passes below the toe of the failed mass. Observations from earlier manned submersible dives suggest that the initiation of the slide was facilitated by secondary faults associated with the Hercynian orogeny and involved Palaeozoic shales dipping southwards towards the deep basin. Radiocarbon dating of core material, together with the well-dated Marmara sapropel above the chaotically mixed landslide surface, reveal that the latest landslide event occurred about 17 ¹⁴C ka B.P. The uppermost scar of the landslide is found at 250 m and its toe at about 1,200 m below the present sea level. At the time of the slide, the Marmara Sea Basin was lacustrine, with its water level at –85 m. In plan view the landslide has a distinctively triangular shape and the lateral extent of its

toe is about 10 km. Multibeam bathymetric data indicate that the sliding motion probably occurred in two phases: a slower phase affecting the eastern part, characterized by an undulating surface, and a more rapid phase affecting the western part that possibly created tsunami waves. In the seismic sections, older failed slide masses can be clearly identified; these were probably displaced during marine isotopic stage 6 (~127–160 ka B.P.). The front of this buried material is located more than 1.5 km further south of the fault. We used a three-dimensional, Green's function-based potential theory approach, rather than shallow-water equations commonly used in conventional tsunami simulations. The solution algorithm is based on a source-sink formulation and an integral equation. The results indicate that the maximum height of the tsunami in the Çınarcık Basin could have reached about half the average thickness of the sliding mass over a lateral extent of 7 km. Assuming an average thickness of 30 m for the landslide, and considering that the water level at 17 ka B.P. was at about –85 m, the modelling shows that the maximum wave height generated by the slide would have been about 15–17 m.

Introduction

Since the catastrophic tsunami event of 2004, which killed over a quarter of a million people along the shores of states bordering the north-eastern Indian Ocean, tsunami risk assessments and “tidal-wave” simulations have been given high priority by many governments the world over. While tsunami warning systems are well established in most states bordering the Pacific Ocean where tsunami events occur relatively frequently, such systems are lacking altogether in regions where such catastrophes are so rare as to have

M. S. Özeren (✉) · M. N. Çağatay · A. M. C. Şengör · N. Görür ·
K. Eriş
Istanbul Technical University (ITU)
EMCOL and Department of Geology Faculty of Mining,
Ayazağa,
80626 Istanbul, Turkey
e-mail: ozerens@itu.edu.tr

N. Postacıoğlu
Department of Physics, Istanbul Technical University (ITU),
Ayazağa,
80626 Istanbul, Turkey

escaped human memory. In this respect, the 2004 Indian Ocean tsunami has taught mankind a sore lesson.

The simulation of tsunami waves, however, is wrought with many difficulties. Thus, in the case of tsunamis generated by submarine landslides, it is often difficult to relate the observational data to the hydrodynamic phenomenon, even in contemporary times. The 1998 Papua New Guinea tsunami, which killed more than 2,000 people, was the first submarine landslide-generated tsunami for which the seismological (and, later, marine geophysical) data were of sufficiently good quality to enable researchers to combine various aspects of the theory with data (Geist 2000; Okal and Synolakis 2001; Tappin et al. 2001). As a fluid mechanical problem, submarine landslide-generated tsunamis have been approached from various angles. Especially during the last two decades, numerical (Harbitz 1992; Harbitz et al. 1993; Grilli and Horillo 1997; Grilli and Watts 1999; Grilli et al. 2002; Hébert et al. 2002; Bondevik et al. 2005; Pareschi et al. 2006, 2007; Tinti et al. 2006a, b), analytical (Pelinozsky and Poplavsky 1996; Ward 2001) and experimental studies (Watts 1998, 2000; Watts et al. 2003; Liu et al. 2005) have helped to improve our understanding of this phenomenon.

The Sea of Marmara (SoM) in NW Turkey is a case in point. It is a seismically very active region and, hence, a prime candidate for tsunami occurrences, although few serious incidents have been recorded in living memory. Indeed,

historical reports and instrumental records of earthquake activity in the SoM region show that about 300 earthquakes ($M > 6$) have occurred during the last 4,000 years (Soysal et al. 1981; Ambraseys and Finkel 1991). More recently, in their analysis of earthquake recurrence times in the SoM, Utkucu et al. (2009) came to the conclusion that the region could expect a large earthquake within the next two decades.

The slopes of the SoM are very steep (15–25°) and marked by several submarine canyons and landslide scars (Gazioğlu et al. 2002). The easternmost Çınarcık Basin is the largest and deepest of the three basins (max. 1,276 m), its slopes exceeding 20°. The most significant palaeo-landslide in this region is the Tuzla submarine mass failure located on the north-eastern slope of the Çınarcık Basin, south of the town of Tuzla (Baş and Alpar 2003; Gazioğlu et al. 2005; Figs. 1 and 2). An engineering geological assessment of this landslide and its surroundings was made by Gökçeoğlu et al. (2009). This and many other landslides in the SoM were probably triggered by earthquakes along the North Anatolian Fault. The records of these earthquakes and associated mass flows are found in the form of turbidites and homogenites in the deep Marmara basins (Cita and Rimoldi 1997; Sarı and Çağatay 2006; McHugh et al. 2006; Beck et al. 2007).

The tsunami problem threatening the SoM has been addressed in several studies, mostly focusing on the 1999 Izmit earthquake and the associated tsunami run-up

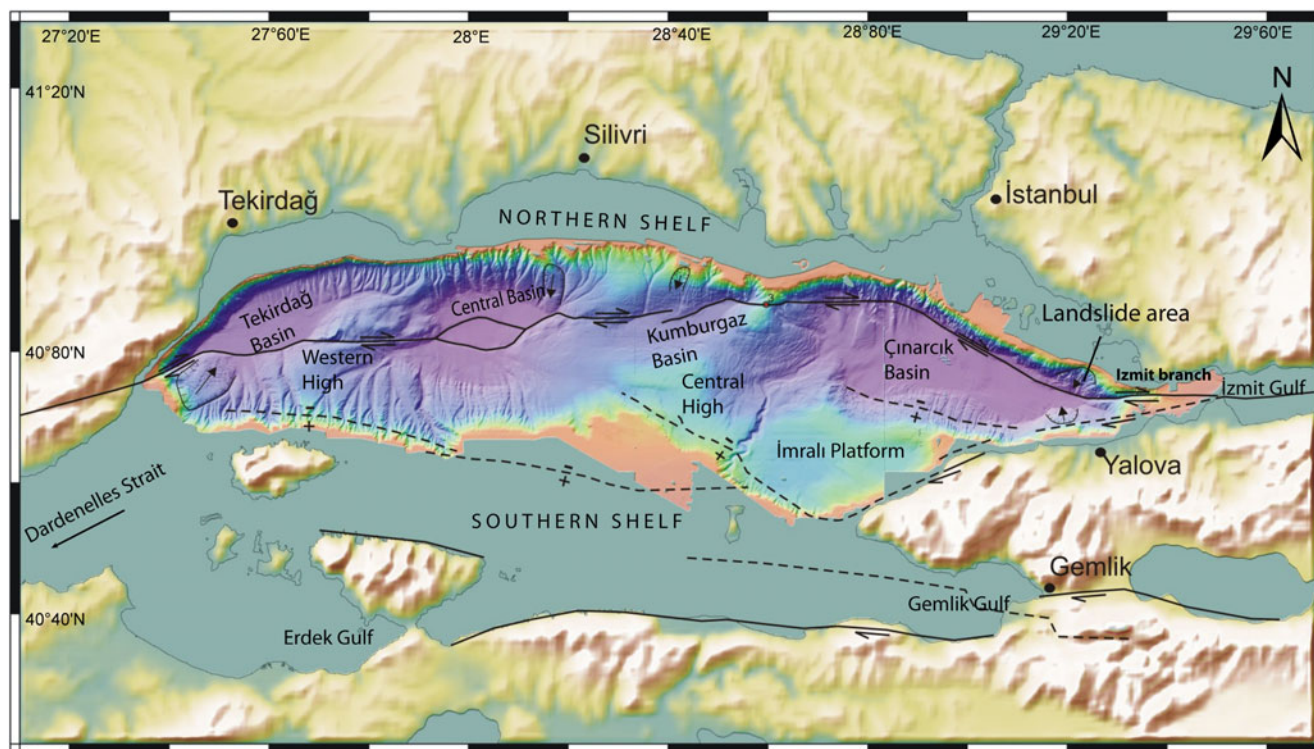
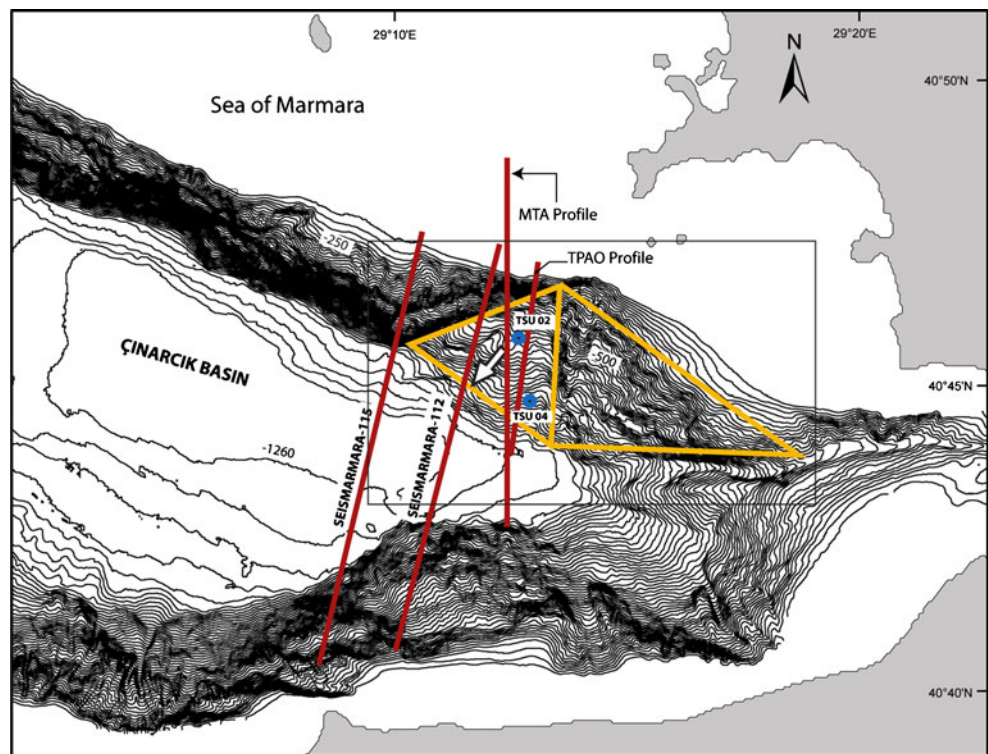


Fig. 1 Location map and generalized physiography of the Sea of Marmara. The landslide discussed in this paper is located in the easternmost part of the Çınarcık Basin

Fig. 2 Multibeam bathymetric map of the study area showing the locations of the four seismic lines MTA, TPAO, SEISMARMARA-112 and -115 displayed in Figs. 3, 4, 5 and 12 respectively, as well as of cores TSU-2 and TSU-4. *Rectangle* Area affected by the landslide, *white arrow* direction in which the simulation of the sliding mass and the resulting tsunami waves was centred. The fast- and slow-moving parts of the landslide are roughly demarcated by the *yellow triangles* to the left and right respectively



(Yalçınır et al. 2000, 2002; Alpar et al. 2001; Altınok et al. 2001, 2003; Hébert et al. 2005; Tinti et al. 2006a). In analyzing historical records of the AD 1265 and AD 1935 earthquakes on Marmara Island, Altınok and Alpar (2006) specifically emphasize the fact that “abnormal” sea waves were observed on those occasions. Modelling studies commonly use shallow-water equations for the generation and propagation of tsunami waves. A more recent tsunami modelling study of the Tuzla landslide assumed zero scattering from the scar area, being based on Fourier-Laplace transform source representation methodology (Hayir et al. 2008). This study inherently assumed a sliding motion on a flat surface, with a hypothetical slide that would presumably have started at the bottom of the current scar, rather than higher up on the slope, as is considered in the present study.

In this paper, multibeam bathymetric as well as seismic and core stratigraphic data related to the submarine landslide off the Tuzla Peninsula on the north-eastern slope of the Çınarcık Basin are assessed. In addition, the submarine-based findings are related to the geology on the adjacent land. Finally, a mathematical modelling analysis investigates the dimensions and deep-water propagation characteristics of tsunami waves that could potentially have been triggered by the submarine mass movement. A run-up analysis was beyond the reach of the linear scheme used in this study and, thus, no calculations were done on wave propagation over the shallow shelves.

The main objectives of the paper are, firstly, to characterize the landslide with its morphology, lithology and chronology, and its possible mechanics and, secondly, to understand the main characteristics of the tsunami wave field that may have been generated by the landslide in a series of mathematical simulations.

Marine geological setting

Marmara Sea

The Sea of Marmara is a tectonically active basin situated between the branches of the North Anatolian Fault (NAF). It has a relatively broad shelf (max. 45 km) in the south and a narrow one (max. 20 km) in the north, the shelf break being located at a water depth of about 100 m (Fig. 1). It comprises three rhomboidal or wedge-shaped basins that reach a maximum depth of 1,280 m, these being the Tekirdag, Central and Çınarcık basins. This morphology is determined by the interaction of the dextral strike-slip tectonics of the NAF (McKenzie 1972; Şengör 1979; Şengör et al. 1985, 2004; Barka and Kadinsky-Cade 1988; Görür et al. 1997; Çağatay et al. 2000a; Demirbağ et al. 2003; Yılmaz et al. 2009). The NAF subdivides into three branches at about 31°E, approx. 100 km east of the Gulf of İzmit. The northern branch is the most active (cf. the Main Marmara Fault of Le Pichon et al. 2001; also

see Gökaşan et al. 2002, 2003), and extends through the Sea of Marmara to eventually connect with the Gulf of Saros and the North Aegean Trough (Ustaömer et al. 2008).

Çınarcık Basin

The Çınarcık Basin is the largest of the deep SoM basins (Fig. 1), having a sediment fill of about 6 km (Carton et al. 2007). The floor of this wedge-shaped basin covers an area of 810 km². The basin is bound in the west by the transpressive “eastern ridge” and in the east by the İzmit Gulf. The northern margin of the basin commonly dips at 20–26°, and is delimited near its base by the very active northern branch of the NAF, the Main Marmara Fault, mainly in the form of a strike-slip component (Okay et al. 2000; İmren et al. 2001; Le Pichon et al. 2001). The deepest spot is in the north-eastern sector of the basin (–1,276 m), but there is another important subsidence zone to the northwest. The southern shelf has a width of 30–35 km, and includes E-W- and ESE-WNW-trending, north-dipping normal faults and half-grabens created by this faulting (Smith et al. 1995). Because sediments brought by rivers such as the Susurluk and Gönen accumulate mainly in the half-grabens of the southern shelf, the thickness of Holocene sediments is greater here than on the northern shelf. However, during the last glacial and early phase of deglaciation when the shelf area was exposed, fluvial sediments were transported directly into the deep basin, resulting in sedimentation rates of 3–4 m/1,000 years (Çağatay et al. 2000b).

Chronostratigraphy and sedimentology of Late Quaternary sediments

To assess the timing of the landslide, an outline of the local stratigraphy is appropriate. Previous sediment core studies in the SoM have identified two principal Late Quaternary stratigraphic units (Çağatay et al. 2000b): an upper marine unit (unit 1) and a lower lacustrine unit (unit 2). The boundary separating the two units has been dated at 12 ka ¹⁴C years B.P. (uncalib. age). Unit 1 consists of green mud and contains a rich fauna of Mediterranean euryhaline molluscs, echinoids and foraminifers (Çağatay et al. 2000b; Aksu et al. 2002; Kaminski et al. 2002). This unit includes two sapropelic layers, rich in organic matter (maximum organic carbon content of 3.4 dry wt%; Çağatay et al. 1999, 2000b; Tolun et al. 2002). Radiocarbon dating has shown that the lower sapropelic layer was deposited between 10,600 and 6,400 years B.P. and the upper one between 4,750 and 3,200 years B.P.

Lacustrine unit 2 was deposited in areas deeper than about –85 m. On the outer shelf it is composed of sandy and silty mud with colours changing from grey to dark

grey. In the deeper parts the unit also locally includes iron monosulphide reduction bands. On the shelf edge and upper slope, the unit includes an assemblage of fresh- to brackish-water molluscs. On the pressure ridges where the sedimentation rate is low (about 30 cm/1,000 years; Çağatay, unpublished data), a 5-cm-thick volcanic ash layer has been identified (Çağatay et al. 2000b; Wulf et al. 2002). Based on its rhyodacitic composition, stratigraphic position, and the results of deep-sea core studies in the eastern Mediterranean, this ash layer has been correlated by Çağatay et al. (2000b) and Wulf et al. (2002) with the Y-2 volcanic ash layer of the Cape Riva eruption on Santorini island, dated at 18 ka ¹⁴C B.P. (22 ka calib.) in Eastern Mediterranean cores (Keller et al. 1978; Cita and Aloisi 2000).

Material and methods

Geological and geophysical methods

The multibeam bathymetric map (Fig. 2) was obtained using a SIMRAD EM300 multibeam echo sounder onboard the RV *Le Suroit* in 2000 (Le Pichon et al. 2001).

Four airgun multichannel seismic reflection lines crossing the landslide are assessed in this study (cf. Fig. 2). Seismic line MTA was obtained onboard the RV *MTA-Sismik-1* in 2001, and processed by Emin Demirbağ and Caner İmren at ITU’s Nezihi Canitez Seismic Processing Laboratory. The number of channels was 84, and the 6-s record was sampled at 2-ms intervals. Shot interval was 50 m and the CDP (common depth point) interval 6.25 m.

Seismic line TPAO is a multichannel airgun profile from the database of the Turkish Petroleum Company (TPAO). In this case, the number of channels was 48, and the 5-s record was sampled at 4-ms intervals. Shot and CDP intervals were 25 and 12.5 m respectively (Siyako et al. 2000).

Seismic lines SeisMarmara-112 and -115 are from the 2001 SeisMarmara survey (Carton et al. 2007). These were shot aboard the RV *Nadir* equipped with a 4.5-km-long streamer and a 2,900 cubic inch airgun array.

Two gravity cores, TSU-2 and TSU-4, were recovered from board the RV *MTA-Sismik-1* in 2001 at water depths of 761 and 988 m on the submarine landslide on the north-eastern slope of the Çınarcık Basin (Fig. 2). The cores were described visually and sampled at 10-cm intervals, the samples being subsequently analyzed for organic carbon content using the Walkey-Blake method (Gaudette et al. 1974; Loring and Rantala 1992).

One sample from core TSU-4, which penetrated the landslide material below the normal Late Quaternary sedimentary sequence of the SoM, was dated using AMS

(accelerator mass spectrometry) radiocarbon dating at the University of Arizona’s NSF AMS facility. Because of the lack of datable material near the base of the undisturbed sediment in contact with the disturbed deposit below, the total carbonate carbon in the sample was dated. The age was calculated in ¹⁴C years B.P., corrected for ¹³C, and the error expressed as ±1σ.

In 2007 the MARNAUT cruise aboard the RV *L’Atalante* (cf. Géli et al. 2008) was instrumental in providing data enabling us to establish links between the onshore and offshore geology of the Istanbul region, including visual inspections and in situ samplings of bedrock in the slide scar using the submersible *Nautile* provided by IFREMER, France.

Mathematical modelling

In the modelling of landslide tsunamis, the sliding mass is traditionally considered to be an *equivalent* rigid sliding block. This simple and practical approach using Green’s functions (Pelinovsky and Poplavsky 1996) works well enough, provided that one is interested only in the first-order characteristics of the dispersive wave field (Ward 2001). The principal factors that determine the maximum amplitude and shape of the wave are the thickness and the width of the sliding mass, and its velocity-depth history, which depends on the geometrical form of the surface it slides on, the ratio between the density of seawater and that of the sliding mass, and the friction conditions influencing the acceleration of the mass. A short summary of the mathematical technique applied in modelling the surface gravity waves that result from the landslide movement is given below, the full derivation of the mathematical technique being given in Özeren et al. (2007) and Postacioglu and Özeren (2008).

The present study makes use of Green’s functions, the focus being on the linear problem, nonlinear issues such as numerical calculations of the tsunami wave run-up being beyond the scope of this paper. The nonlinearities that are related to the generation and propagation phases (Yalçiner and Pelinovsky 2007) are not critical for our particular generation and early propagation problem (see Postacioglu and Özeren 2008). This means that the convective terms in the Navier-Stokes equations that govern the fluid motion can be neglected. We used a deep-water approach to model the landslide tsunami because the triggering mechanism for the waves (the landslide) is very localized in space, as opposed to the laterally very large-scale fault ruptures that create conventional tsunamis. In the depth range we are interested in, the water column acts as a kind of low-pass filter; hence, very detailed shape information of the mass displaced during the landslide is not critical for calculations of the wave field at the water surface.

We chose a semi-spectral method that, under the linearity assumption, enabled us to calculate the dispersive wave field in three dimensions using a semi-analytical approach, with scattering from the bathymetry in the presence of a mass that is sliding on a fairly steep slope. In this context, it is interesting to note that Kilinc et al. (2009) found no significant differences between dispersion and non-dispersion solutions for tsunami propagation in the SoM.

Under the assumption of an inviscid and incompressible fluid, the system to be solved simply reduces to the Laplace equation for the velocity potential φ in the fluid domain at all times:

$$\nabla^2\phi(x, y, z, t) = 0 \tag{1}$$

subject to the kinematic condition on the sea bottom

$$\partial_n\varphi = 0 \tag{2}$$

where n indicates the normal vector into the fluid anywhere on the sea bottom. The thickness of the sliding block was taken to be much less than the water depth, satisfying the following two conditions on the free surface:

$$p = \rho_D \left(\frac{\partial\phi}{\partial t} \Big|_{z=0} - g\eta \right) \tag{3}$$

$$\frac{\partial\phi}{\partial z} \Big|_{z=0} = \frac{\partial\eta}{\partial t} \tag{4}$$

where ρ_D is the density of the fluid, g the acceleration due to gravity and η the departure from the undisturbed free surface. For details of the solution methodology, the reader is referred to Postacioglu and Özeren (2008).

The motion of the landslide itself was modelled using the following differential equation:

$$m_b\ddot{s}_b = -\frac{dU_g}{ds} - \frac{1}{2}HW\rho_Dc_d\dot{s}_b^2 - F_C \tag{5}$$

where U_g is the gravitational potential energy of the block and F_C the basal friction force. Evaluating U_g accounts for buoyancy, in that U_g is defined as

$$U_g = V \times z(s) \times \frac{\rho_B - \rho_D}{\rho_D} g \tag{6}$$

where V is the volume of the block, $z(s)$ the depth of the position on the trajectory, ρ_B the block density and ρ_D the density of seawater (the latter taken to be 1 and 2.7 g/cm³ respectively); the last term of the equation represents gravity taken to be 10 m/s². In Eq. 5, m_b is the mass of the sliding block, c_d the hydrodynamic drag coefficient and s the curvilinear coordinate along the trajectory, the dots in the equation indicating derivatives with respect to time. *W*

is the width and H the thickness of the sliding block. The last term in Eq. 5 is given as

$$F_C = \frac{\rho_B - \rho_D}{\rho_D} c_m \cos \theta \quad (7)$$

where c_m is the Coulomb friction coefficient and θ the local slope angle. This is simply Newton's law of motion, taking into account the friction, buoyancy forces and the effect of the added mass. The reader is referred to Watts (1998, 2000) for experimental studies in which these effects are explained in more detail.

Results

Slide morphology, internal structure and stratigraphy

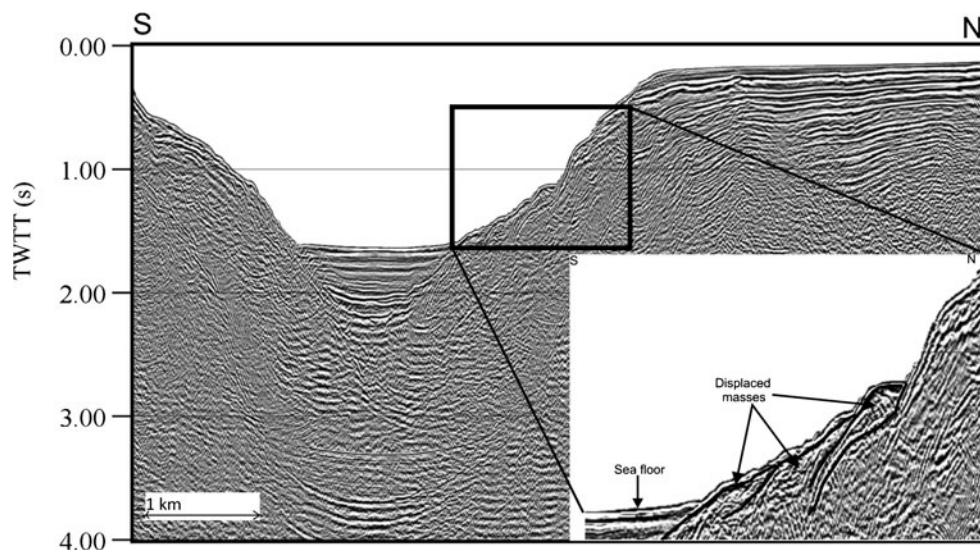
The Tuzla mass failure is a very large submarine landslide along the north-eastern continental slope of the Çınarcık Basin. It has a roughly triangular shape, the shelf-side vertices being 8–9 km long on each side of the slope (Fig. 2). The displaced mass, which is clearly visible on the multibeam bathymetry and in the multichannel seismic cross sections, has an average thickness of approx. 30–40 m (assuming a seismic velocity of about 1,480 m/s for the shallow sediments) and displays compressional features in the frontal zone (Figs. 3, 4).

The multichannel profiles from the SeisMarmara project also reveal older mass wasting events besides the late glacial Tuzla landslide. As evident from Fig. 5, the upper surface of the lens-shaped, half-buried part of this older mass failure connects to a basin-wide transparent reflector (indicated with a black arrow in Fig. 5). Considering the depth at which it occurs, the lowest frontal part of this slide is unlikely to be related to the Tuzla landslide.

The large size of the more recent submarine landslide suggests that it has probably been triggered by a large earthquake. Its overall triangular shape can be subdivided into two smaller triangles that are characterized by two very distinct morphologies (Fig. 2). The eastern one has a gentler average slope with a staircase-like (hummocky) topography, and is bounded in the east by the Izmit branch (extending from the Gulf of İzmit) of the Main Marmara Fault. There are neither cores nor seismic sections available from this part of the landslide, which makes an assessment of its mechanics difficult. The western part, on the other hand, has very steep bathymetric gradients, the landslide material and the scar having slope angles greater than 25°. This indicates that the landslide occurred relatively fast, possibly as a tsunamogenic gravity failure. However, we do not rule out that several small-volume landslides may have occurred on either side of the scar since the late glacial event.

Cores TSU-02 and TSU-04 are located in the western part of the slide, the former from a water depth of 761 m, the latter from 988 m (cf. Fig. 2). Both cores reveal a late glacial to Holocene stratigraphic sequence typical of the SoM (Figs. 6, 7). Judging from the position of the Marmara sapropel in the two cores, the shallower core (TSU-02), in spite of its greater length (2.55 m), evidently covers a shorter time span than does the deeper core (TSU-04), which is only 1.55 m long. From the stratigraphy it is clear that core TSU-02 did not penetrate into the deformed slide deposit. Core TSU-04, by contrast, can be subdivided into an 87-cm-thick marine sequence above the sapropel, and a 58-cm-thick lacustrine sequence below the sapropel. At its base, the core penetrated about 5 cm into a chaotic mixture comprising angular shale clasts, angular pebbles, and a sandstone block in a sandy mud matrix that evidently represents the top of the deformed slide body. This

Fig. 3 Multichannel airgun seismic profile MTA (cf. Fig. 2) obtained onboard the RV *MTA-Sismik-1*. Landslide masses are clearly seen as remoulded material. *TWTT* Two-way travel time



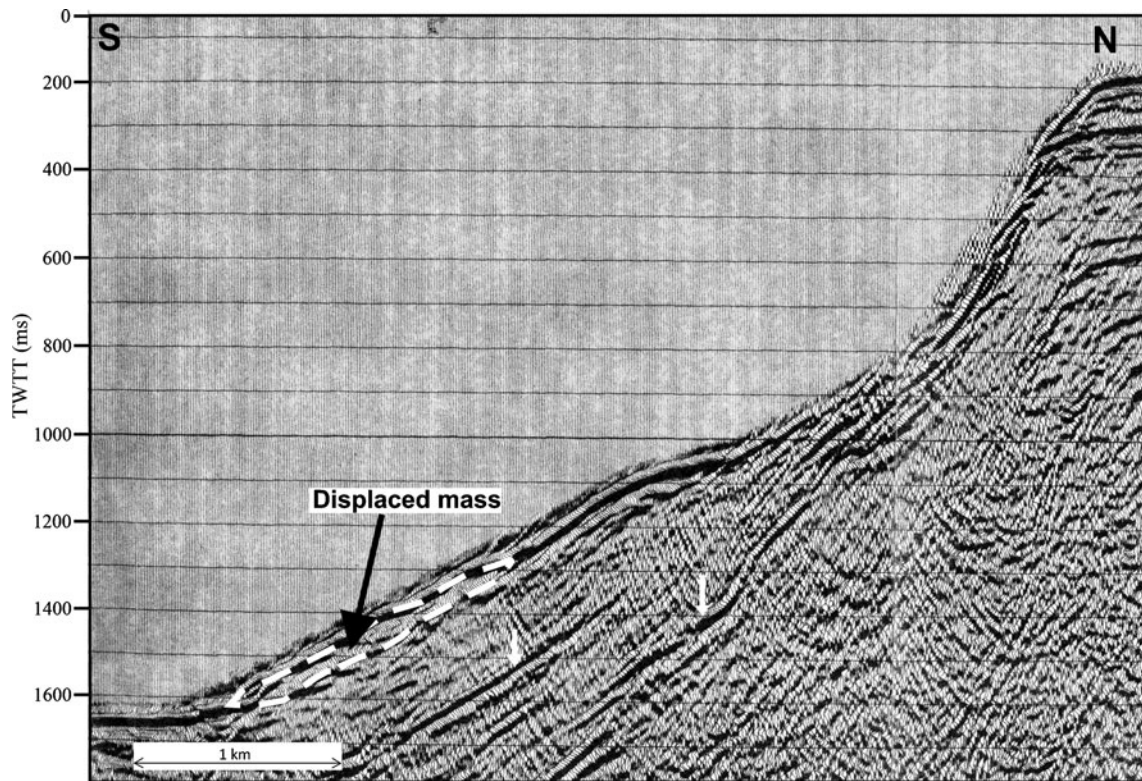


Fig. 4 Multichannel airgun seismic profile TPAO (cf. Fig. 2). The main scarp, the displaced mass (*black/white line*) and some of the flow deposits at the toe of the landslide can be clearly recognised. *White arrows* Glide planes, *TWTT* two-way travel time

sequence includes the characteristic lower Marmara sapropel unit showing high contents of organic carbon (>1.5 wt%) and the lacustrine/marine transition that have previously been dated at 10,600–6,400 and 12,000 ¹⁴C years B.P. respectively (Çağatay et al. 2000b). The radiocarbon dating on the “total” carbonate carbon in a sample from 148 to 149 cm core depth, i.e. immediately above the landslide material, yielded an age of 23,400±170 ka B.P. This age is certainly too old for

the landslide event because this material would include “radiogenically dead” carbon from detrital carbonate. The fact that the 18 (uncal.) ka B.P. Santorini ash layer is absent in core TSU-4 indicates that the base of the core is younger than 18 ka (22 ka calib.), the age of the Santorini’s Cape Riva ash (Keller et al. 1978), but older than the lacustrine/marine transition at 12 ka B.P. (Çağatay et al. 2000b). Considering that the age of the unit 1/unit 2 boundary at

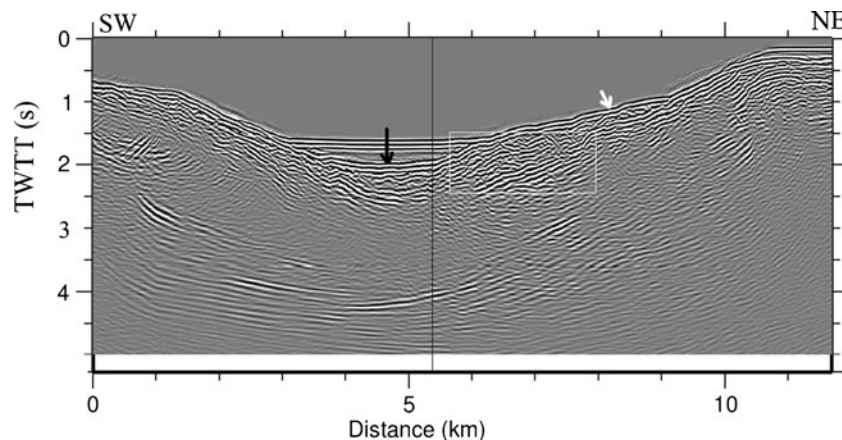
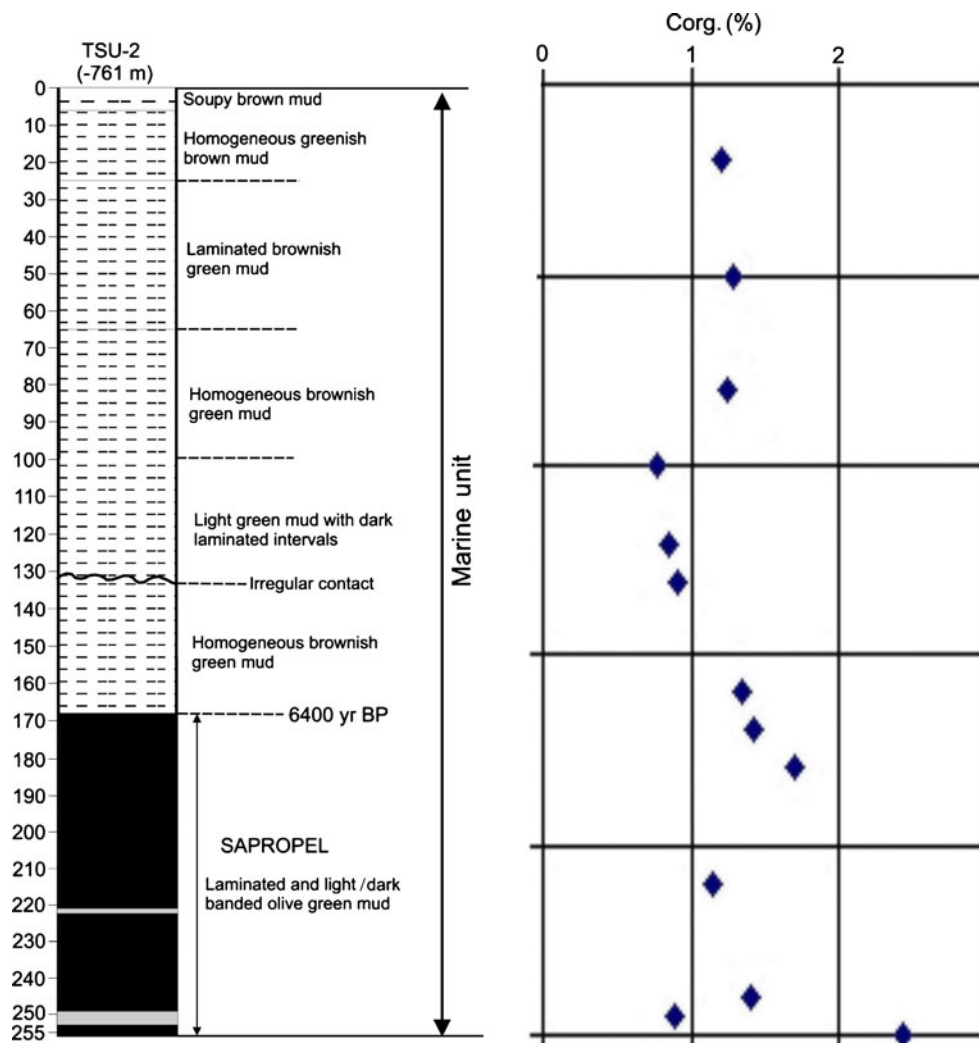


Fig. 5 SeisMarmara multichannel seismic section number 112 (cf. Fig. 2). *White arrow* Remoulded material corresponding to the late glacial slide, *white rectangle* older, lens-shaped buried landslide masses, which probably comprise several landslides that occurred

during MIS 6 or immediately prior to it. Note that the internal reflections beneath the transparent deposits in the basin centre (*black arrow*) merge with the upper surface of the older landslide masses. *TWTT* Two-way travel time

Fig. 6 Stratigraphy and organic carbon (Corg) profile of core TSU-2, revealing the presence of a sapropel layer with Corg values reaching more than 1.5 dry wt% below a core depth of about 180 cm. Note the ^{14}C -dated horizon



87 cm below seafloor is 12 ka, and assuming a typical sedimentation rate of 10 cm/1,000 years for unit 2 on the slope (Çağatay, unpublished data), the age of the slide is calculated to be about 17 ka B.P. From these observations, it is clear that the late glacial-Holocene sequence has been deposited after the submarine landslide.

Stratigraphy and structure of onshore and offshore deposits and their relation to the kinematics of the landslide

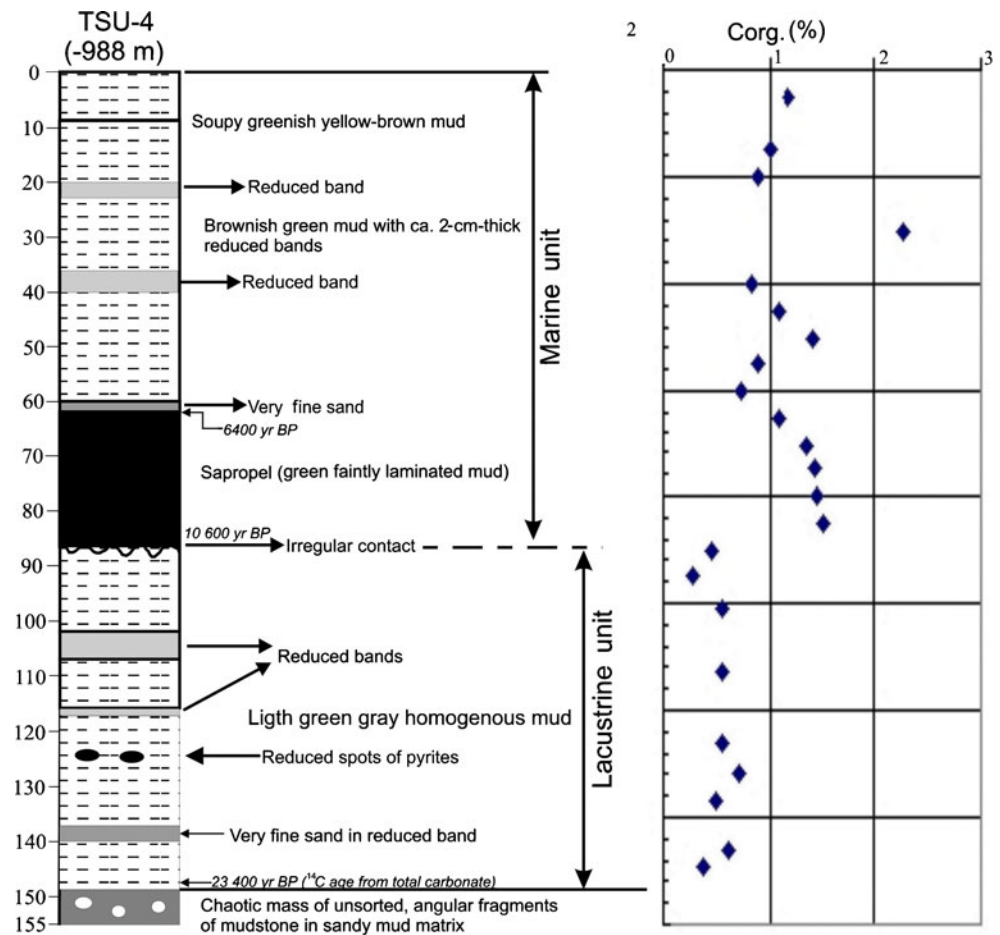
The Palaeozoic of the Istanbul region consists of an approx. 10-km-thick Atlantic-type continental margin sedimentary package spanning an age interval from the Late Ordovician to Early Carboniferous (Figs. 8, 9; Şengör and Özgül 2009). The succession has a west-vergent imbricated structure that forms the outermost part of a marginal fold and thrust belt (Fig. 10). In the east, the wide arkosic terrain seems to represent at least four major tectonic slices. These overrode small patches of discontinuous quartzites, thereby folding and in part imbricating the more continuous Devonian rocks. It would appear that under the Golden

Horn the Carboniferous flysch backthrusts the Devonian and partly also the Carboniferous rocks, most probably forming a triangle-shaped anticline at depth, herein called the Beyoğlu Triangle Zone (Fig. 10). Indeed, it is here that west-dipping shear zones have been observed in the Carboniferous sedimentary rocks (Ketin and Guner 1988).

The thrusts have a west-concave shape and the resulting concavity is locally accentuated by west-northwest-striking tear faults. It seems that the southern shoreline of the Istanbul region is closely paralleled by such faults, a remarkable example of which can be seen on the island of Büyükada (Prinkipio of the Princes' Islands of Byzantine times; Ketin 1953). The tear faults are all right-lateral and bring the Early Palaeozoic rocks of the Princes' Islands into strike continuity with much younger rocks of the Kocaeli (Bithynian) Peninsula.

The results of the *Nautilie* dives during the MARNAUT cruise in 2007 are in agreement with this general interpretation. During *Nautilie* dive no. 1652, a white orthoquartzite unmistakably part of the Aydos Formation (Fig. 9) was encountered at a depth of some 1,100+ m

Fig. 7 Stratigraphy and organic carbon (Corg) profile of core TSU-4, revealing the presence of a sapropel layer with Corg values reaching more than 1.5 dry wt% at core depths of 62–86 cm. Note the ¹⁴C-dated horizons



(Şengör, unpublished data). Immediately above the quartzite, a fairly tightly folded black shale sequence was observed that persisted to a depth of 900 m. In places, this shale was silty but rarely sandy. Bed thicknesses increased bathymetrically upwards but never exceeded 20–30 cm. Up to a depth of some 1,050 m, the dip directions were persistently towards the south (i.e. towards the centre of the Çınarcık Basin) and southeast, with dip values varying between 30° and 45°. At shallower water depths, the dip changed towards the east with similar dip values. At a depth of 1,000 m, a fault striking N30W was observed. Farther west, during *Nautila* dive no. 1658 (30th May 2007), a black shale sample was recovered at a depth of about 1,100 m (Görür, unpublished data), this being in excellent agreement with the observations of Şengör (cf. above).

Tsunami wave modelling

In the tsunami simulations, certain characteristics of the landslide, such as the type of mass movement (sliding motion on a slope and rotational failure of the sediments) and the mass dimensions, were changed stepwise in a series of case studies in order to test the responses. At this point it

must again be emphasized that the ambiguities related to the mechanics, and the uncertainties regarding the geometry of the landslide prevented the formulation of realistic assumptions for the bottom boundary conditions of the model. The aim therefore was to capture the fundamental, first-order characteristics of the wave field, given the geometrical scales of the triggering mass failure as deduced from the bathymetry and the seismic data. As explained above, the water level at the time of the landslide (about 17 ka B.P.) was about 85 m lower than the present-day level.

In order to evaluate the effects of various landslide parameters on the tsunami wave height, we performed simulation runs by varying the slide width, hydrodynamic friction coefficient c_d and Coulomb coefficient c_m . In most quantitative studies of submarine landslides, c_m is either assumed to be zero (e.g. Watts et al. 2003) or given a small value such as 0.02 (e.g. Fine et al. 2003). Establishing this value with precision for a given landslide scenario is difficult but numerical studies of submarine debris flows such as that of Imran et al. (2001) have shown that such small values of c_m are indeed realistic. We performed runs with c_m values of 0.0, 0.025 and 0.050. For c_d , the hydrodynamic friction coefficient, we used values of 1.0 and 1.5. Given our rectangular block assumption, these

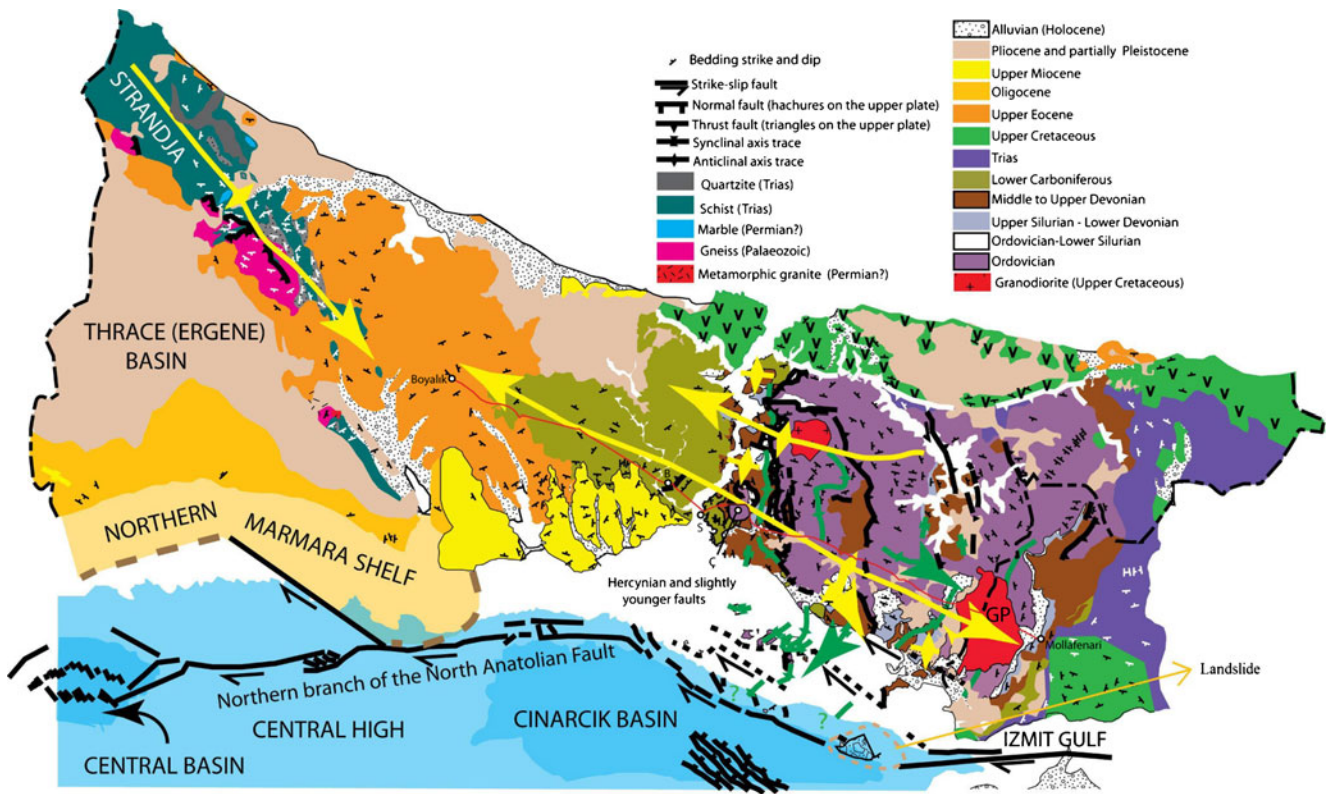


Fig. 8 Simplified geological map of the Istanbul region (modified after Şengör and Özgül 2009), the landslide locality being indicated at the lower right. Also given are the locations of the Beyoğlu, Çamlıca

and Salacak districts of the City of Istanbul shown in the cross section in Fig. 10 (B, Ç and S respectively, white circles). GP Gebze Pluton

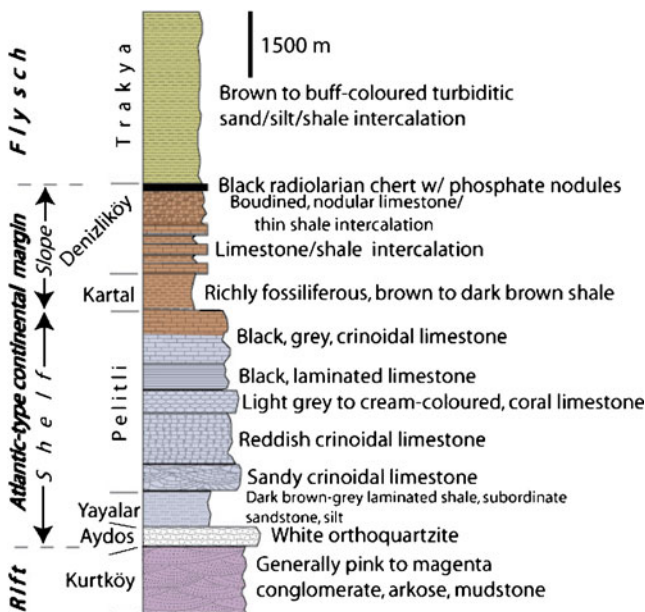
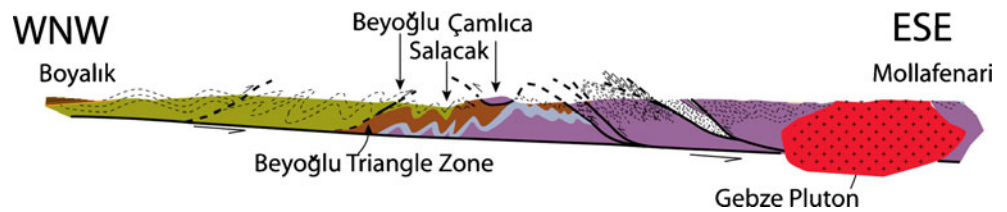


Fig. 9 Simplified stratigraphy of the Istanbul Zone (modified after Şengör and Özgül 2009)

values are plausible. For each Coulomb and hydrodynamic friction coefficient combination, we did runs for slide width values of 5 and 7 km. The maximum wave heights at the instance when the front of the slide reaches the toe of the slope are given in Table 1. As one might have expected, the effect of the Coulomb coefficient is quite dramatic, the wave heights more than doubling when c_m is changed from 0.050 to zero. This effect is somewhat more pronounced for the narrower (5-km-wide) slide. This is not surprising because the geometric spreading factor decreases as the width increases. For very small values of c_m , the maximum wave height is invariably more than half the thickness of the sliding mass within the hydrodynamic friction bounds mentioned above.

In Fig. 11a–f, the generation of the waves and their propagation as a function of time are illustrated in free-surface plots for the particular case in which we assumed zero basal friction and $c_d=1$, and set the width of the landslide at 7 km. Both a dispersive character and lateral spreading are apparent. The wave train develops a negative bulge behind the front as it propagates over the deep basin (a typical feature observed also in experimental studies such as that by Liu et al. 2005) towards the northern coast of the Armutlu Peninsula. The images are meant to convey the physical scale of the wave field in relation to its shape

Fig. 10 Simplified geological WNW–ESE cross section of the Istanbul Zone (modified after Şengör and Özgül 2009). Beyoğlu, Çamlıca, Salacak, etc. are districts of the City of Istanbul



evolution, rather than claiming to be a precise representation of a past tsunami event. The maximum wave height in this particular case is 0.58 times the thickness of the sliding mass (indicating a 16–17 m maximum pre-run-up height over the deep water for an average landslide thickness of 30 m). For slide blocks having a width twice as large, this factor increases to about 0.68 for the same bathymetry, the maximum wave height in this case thus amounting to about 20–21 m. In all simulations, the scattering of the waves for the entire duration of the simulation was taken into account. Not surprisingly, the amplitudes of the waves that propagate towards the south (thus, in the direction of the sliding motion) are larger than for those propagating towards the north. The northward-propagating waves would reach the shallow shelf early in their evolution and, as they constitute a coastal flooding threat, they cannot be ignored. It is also important to remember here that the asymptotic value of the maximum wave height (calculated for a given trajectory length) is reached quicker for smaller slide block widths and shorter slide trajectories.

We ran simulations assuming a bathymetry that is 85 m shallower than that of today, and found the maximum wave heights in this case to be about 11% higher. This increase is not surprising, as the starting position of the landslide is closer to the sea surface and, consequently, higher sliding

velocities are reached when the front of the sliding mass is still at shallower depths.

Discussion

Slide morphology, internal structure and stratigraphy

The steep bathymetric gradients and the proximity of the Main Marmara Fault to the northern slopes bounding the Marmara basins constitute an ideal setting for submarine landslides (Zitter et al. 2008). The wiggly shape of the remoulded material at the slide front representing compressional features (Hampton and Locat 1996; Shanmugam 2006; Figs. 3, 4) typically resembles that obtained in numerical simulations where landslide material is treated as a Bingham fluid (Imran et al. 2001; Masson et al. 2006).

Given the very large volume of displaced material in the older slide that underlies the Tuzla slide, it is unlikely that it is a product of a single landslide. In two profiles (SeisMarmara-113 and 114) located to the west of the slide reported by Carton et al. (2007), the same feature is visible, yet the sediments seem to be more disturbed and the connection between the frontal landslide material and the basin-wide reflector becomes more difficult to trace. The obvious question here concerns the identity of the basin-wide reflector that seems to correlate with the last of these large, older landslide masses. This reflector is well known (e.g. Parke et al. 1999, 2002; Okay et al. 2000) and marks the lower limit of the so-called *upper sequence*. Carton et al. (2007) identified the same reflector (indicated by an orange colour in their Fig. 4) overlain by sediments having a low P-velocity (1.5 to 1.7 km/s). Figure 12 shows profile SeisMarmara-115 of Carton et al. (2007) with the reflector highlighted by the same orange colour. Carton et al. (2007) relate the deformation solely to the existence of two diverging faults bounding the basin from the north—one at the toe of the present scar, the other some distance further south (Fig. 12)—but do not mention the buried landslide masses. However, immediately above the orange reflector, i.e. within the *upper sequence*, there are two additional reflectors. Assuming an average sedimentation rate of 3–3.5 mm/year in the deep Çınarcık Basin (Çağatay, unpublished data), the part between the orange and dark purple reflectors in Fig. 12

Table 1 Results of simulation runs for various values of c_m , c_d and slide width. Maximum wave heights were normalized in terms of average landslide thickness

Coulomb coefficient (c_m)	Slide width (km)	Hydrodynamic friction (c_d)	Normalized maximum wave height
0.000	5	1.0	0.58
0.025	5	1.0	0.45
0.050	5	1.0	0.30
0.000	5	1.5	0.51
0.025	5	1.5	0.35
0.050	5	1.5	0.23
0.000	7	1.0	0.65
0.025	7	1.0	0.58
0.050	7	1.0	0.36
0.000	7	1.5	0.60
0.025	7	1.5	0.42
0.050	7	1.5	0.29

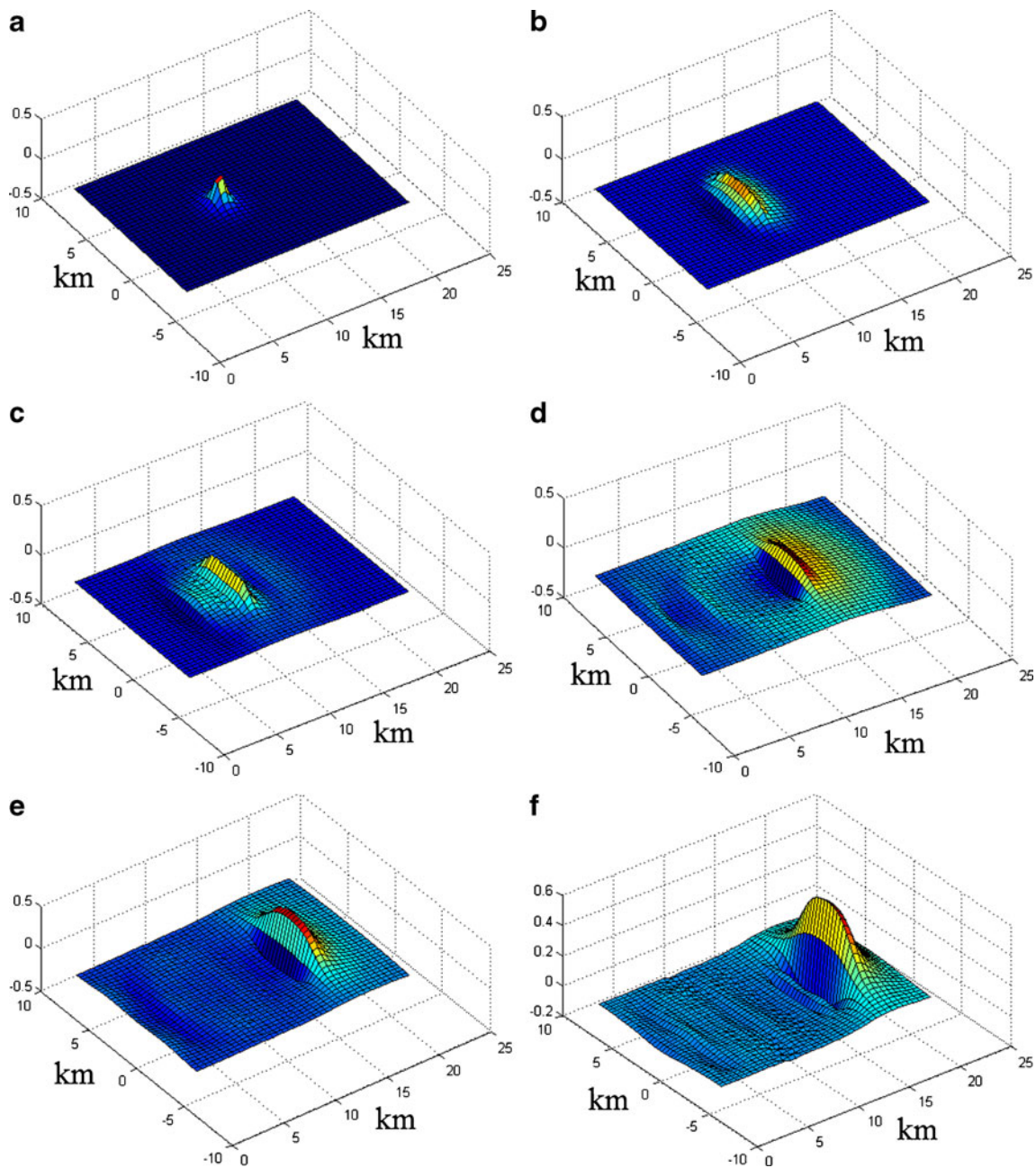


Fig. 11 Time series of a numerically generated tsunami wave above a 7-km-wide submarine landslide, illustrating the evolution of the wave at 0 (a), 44 (b), 88 (c), 187 (d), 242 (e) and 264 s (f). The main wave train travels from *left to right* in the direction (SW) of the white arrow

in Fig. 2. The vertical axis indicates the factor by which the thickness of the sliding block (about 30–35 m, in this case) must be multiplied to obtain the wave height

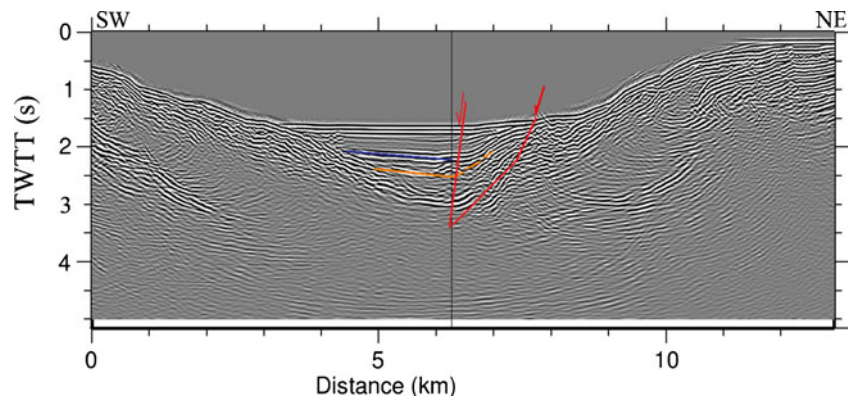
probably corresponds to the marine isotopic stage (MIS) 6 sea-level lowstand (~127–160 ka B.P.).

The overall conclusion, therefore, is that there have probably been a number of large underwater landslides in the same area during MIS 6, the mass failure processes having been facilitated by the subaerial exposure of the shelf.

Stratigraphy, structure and landslide kinematics

The main northern branch of the Northern Anatolian Fault (NAF) enters the SoM in the İzmit Gulf immediately east of the landslide. At this point it makes a bend and carries on as a WNW-ESE-striking transitional fault. This fault branch (sometimes referred to as the Princes' Islands or Adalar

Fig. 12 SeisMarmara multi-channel seismic section number 115 (cf. Fig. 2), located immediately west of the study area: the buried older landslide masses are no longer visible. Note the orange-coloured basin-wide reflector. According to Carton et al. (2007), two faults—one at the toe of the present scarp, the other further south—bound the basin from the north (red arrows). *TWTT* Two-way travel time



branch) is likely to be a strike-slip fault, as suggested by the seismicity near the fault (see focal mechanism inversions of broadband records by Örgülü and Aktar 2001). At present, the right-lateral nature of the Main Marmara Fault and available GPS data from the surrounding region indicate that the kinematics of the SoM is predominantly represented by the principal extensional axis that has, on average, a SW–NE orientation (Le Pichon et al. 2001; Özeren 2002; Nyst and Thatcher 2004).

Based on extensive marine geophysical data, Le Pichon et al. (2001) define the Main Marmara Fault as a relatively simple E–W-striking strike-slip fault. Yet we do not rule out a superimposed normal deformation on the Adalar branch. Indeed, there is a significant lack of consensus on the mechanics of this part of the fault, which is defined by some researchers as a trans-tensional fault (Armijo et al. 2002). With these constraints in mind, we propose that the initial detachment of the slide mass most probably took place on the eastern side, possibly somewhere along the shelf edge of the eastern triangle in Fig. 2 during a large seismic event. Such a mass failure on the eastern side would have been promoted by secondary faults that reactivated Hercynian structures. This tectonically triggered slow movement in the east may then have led to a gravitational instability in the western part, the sliding motion here being accelerated due to the low friction between the Palaeozoic shale beds. A sudden change in the pore pressure due to the earthquake may also have played a role in the process.

The data therefore suggest that at least the western part of the slide is underlain by south- and southeast-dipping lower Silurian black shales that are susceptible to mass wasting in a gravitationally unstable setting. If the onland geological pattern is extrapolated onto the shelf, one would thus encounter younger Palaeozoic rocks in the western part of the slide scar. The WNW-striking dextral tear faults are most probably associated with secondary structures, the N30W-striking fault possibly playing a major role in the process. If so, the eastern border of the slide may be delimited by secondary faults associated with the Hercynian

orogeny, whereas the western border is formed by displaced, south-dipping shales (see also Tur 2007; Gökçeoğlu et al. 2009). In summary, the data suggest that the landslide event took place during a global sea-level lowstand when the water level in the Marmara Basin was about 85 m below the present one, being probably controlled by the bedrock sill depth of the Dardanelles Strait (Çağatay et al. 2003; Polonia et al. 2004; Eriş 2007).

Sediments deposited on the shelf in the wake of the tsunami wave run-up would initially have been subaerially exposed at elevations corresponding to water depths of 65–85 m below the present sea level. The preservation potential of such deposits on a shelf initially exposed to subaerial conditions and subsequently crossed by the postglacial marine transgression from 12 ka B.P. onwards must be considered to be low. Initial fluvial, and possibly even early urbanization in the coastal areas, later followed by wave erosion during the transgression would in all likelihood have destroyed the tsunamogenic deposits.

Tsunami wave modelling

For calibration purposes, we tested our three-dimensional routine, simulating waves created by very wide (literally representing an infinite width, therefore essentially two-dimensional) landslides against direct two-dimensional calculations. The test results were satisfactory in that the simulations converged to the analytically derived asymptotic values corresponding to the purely bi-dimensional results. In addition, the algorithm was compared with the experimental results of Watts (1998, 2000) and Liu et al. (2005) and was found to reproduce the first-order characteristics of the dispersive wave field observed in these laboratory experiments very well. As our simulations assumed linearity, the wave heights were calculated to scale with the thickness of the sliding masses. Hence, any increase in thickness is matched by a corresponding increase in wave height. One of the facets of the linearity assumption is the supposition that the thickness of the landslide is substantially smaller than the water depth. This

assumption is valid in our case, where the sliding motion is *initiated* at a water depth of more than 250 m and the thickness of the slide is deduced to be slightly more than one tenth of this initial depth (cf. this condition is compromised somewhat by the 85-m-shallower, lacustrine Marmara lake level, but there is still a large difference between the slide's thickness and the initial depth). Mathematically, this means that if the solution for the flow field is expanded into a power series in terms of the thickness of the landslide, only the first-order terms are retained as far as the analysis in this article is concerned.

Risk assessment

Such large landslides are demonstrably rare events and they are much less frequent than large earthquakes (Utkucu et al. 2009), yet the proximity of the Main Marmara Fault to the large bathymetric gradient in the north does constitute a tsunami risk for the City of Istanbul as well as the coast to the south. In the case of a landslide to the west of the region under consideration, the Istanbul region would be subject to the waves travelling in the direction opposite to the landslide movement. The test simulations show that, unless the sliding mass is very short (in the direction of propagation), at the presently existing depth range the initial waveforms created by the front and the rear ends of the sliding mass will not cancel each other out in the initial stages of wave evolution. This means that the waves would propagate fairly freely in both directions.

Given this situation, there are a number of issues that need to be investigated in order to assess a future submarine landslide-generated tsunami risk. One problem is the lack of sufficient seismic data across the northern shelf. Pre-existing weak zones may well occur on the shelf and knowledge about their geometry, relative to the slope bounding the Çınarcık Basin and the Main Marmara Fault, would prove useful for such a risk assessment.

During the 2007 MARNAUT campaign, cold seeps, gas bubbles and black patches of varying sizes, bacterial mats and carbonate crusts (as high as several metres in places) were discovered at various locations along the Main Marmara Fault. These features, together with the current tectonic setting, have already been assessed in terms of slope stability (Zitter et al. 2008). Hence, a sudden hydrocarbon gas release from the sediments due to a large earthquake may constitute an additional triggering mechanism for submarine landslides in the region.

It is also important to note that, in terms of “competition” between the pore-fluid pressure and hydrostatic pressure, a glacial low sea-level stand presents a setting that promotes the occurrence of submarine landslides. For the Sea of Marmara, no measurements of pore pressure

exist in the literature. Thus, long-term piezometer monitoring in the high-risk areas is urgently recommended.

Conclusions

In this study of the late glacial Tuzla submarine landslide in the Sea of Marmara, radiocarbon datings on two cores indicate that the landslide occurred about 17 ¹⁴C ka B.P. At this time, the Sea of Marmara was a lake and the water level was at least 85 m lower than today. Manned submersible dives helped to confirm the existence of southward-dipping black shales in the slope area that evidently are an important factor facilitating landslide motion. The black shales are Silurian in age and the onland extrapolation of the submarine-based evidence indicates that the western part of the slide probably consists of younger Palaeozoic rocks. This connection with the land geology also suggests that WNW-striking faults associated with the Hercynian orogeny and their secondary structures may have been reactivated to play an auxiliary role in this slide event.

Multichannel seismic sections from various sources give satisfactory visual evidence of the geometry of the landslide. Another interesting point concerning particular seismic sections from the SeisMarmara project is that these revealed the existence of very large, older landslide masses at the same location, but buried beneath the northern part of the Çınarcık Basin. The upper surface of this mass corresponds with a basin-wide transparent reflector. This possibly indicates that during the MIS 6 sea-level lowstand (~127–160 ka B.P.) there were multiple submarine landslides in the area.

Using the information from the seismic sections, a simple calculation of the velocity of the slide was carried out. Assuming an average slide thickness of about 30 m, and choosing a water level 85 m shallower than today, the semi-spectral hydrodynamic modelling showed that the maximum wave height for the slide would have exceeded 15 m over the deep basin. This finding has important implications for tsunami risk assessments in the Sea of Marmara.

Acknowledgements This study was supported by TUBITAK (Scientific and Technical Research Council of Turkey). We thank Dr. Pierre Henry for several stimulating discussions on chronostratigraphic and mechanical aspects of submarine landslides in the Sea of Marmara. Prof. Emin Demirbağ, and Drs. Caner İmren, Muzaffer Siyako and Satish Singh provided the multichannel seismic sections. We also acknowledge helpful comments from three anonymous reviewers. The ITU Institute of Informatics offered us their computational facilities. Finally, the Turkish Air Force Academy is gratefully acknowledged for drawing our attention to this interesting and important problem.

References

- Aksu AE, Hiscott RN, Kaminski MA, Mudie PJ, Gillespie H, Abrojano T, Yaşar D (2002) Last glacial-Holocene paleoceanography of the Black Sea and Marmara Sea: stable isotopic, foraminiferal and coccolith evidence. *Mar Geol* 190:119–149
- Alpar B, Yalciner AC, Imamura F, Synolakis CE (2001) Determination of probable underwater failures and modeling of tsunami propagation in the Sea of Marmara. In: Proc Int Tsunami Symp ITS 2001, 7–10 August 2001, Seattle, Session 4, no 4-3, pp 535–543
- Altınok Y, Alpar B (2006) Marmara Island earthquakes, of 1265 and 1935; Turkey. *Nat Hazards Earth Syst Sci* 6:999–1006
- Altınok Y, Tinti S, Alpar B, Yalciner AC, Ersoy S, Bortolucci E, Armigliato A (2001) The tsunami of August 17, 1999 in Izmit Bay, Turkey. *Nat Hazards* 24(2):133–146
- Altınok Y, Alpar B, Hébert H, Düzgüt Z, Yalçınar AC (2003) The effects of the Marmara tsunamis on the coastal area and in the Strait of Istanbul. In: Özhan E (ed) Proc 6th Int Conf Mediterranean Coastal Environment MEDCOAST 03, 7–11 October 2003. MEDCOAST Secretariat, Middle East Technical University, Ravenna, Italy, pp 2211–2223
- Ambraseys N, Finkel C (1991) Long-term seismicity of İstanbul and of the Marmara Sea region. *Terra Nova* 3:527–539
- Armijo R, Meyer B, Navaro S, King G, Barka A (2002) Asymmetric slip partitioning in the Sea of Marmara pull-apart: a clue to propagation processes of the North Anatolian Fault? *Terra Nova* 14:80–86
- Barka AA, Kadinsky-Cade K (1988) Strike slip fault geometry in Turkey and its influence on earthquake activity. *Tectonics* 7:663–684
- Baş M, Alpar B (2003) Structural features of the Tuzla region, Istanbul. *Turkish J Mar Sci* 9:97–110
- Beck C, Mercier de Lépinay B, Schneider J-L, Cremer M, Çağatay N, Wendenbaum E, Boutareaud S, Ménot G, Schmidt S, Weber O, Eris K, Armijo R, Meyer B, Pondard N, Gutscher M-A, MARMACORE Cruise Party, Turon J-L, Labeyrie L, Cortijo E, Gallet Y, Bouquerel H, Gorur N, Gervais A, Castera M-H, Londeix L, de Ressaiguier A, Jaouen A (2007) Late Quaternary co-seismic sedimentation in the Sea of Marmara's deep basins. *Sed Geol* 199:65–89
- Bondevik S, Løvholt F, Harbitz CB, Mangerud J, Dawson AG, Svendsen JI (2005) The Storegga slide tsunami—comparing field observations with numerical simulations. *Mar Petrol Geol* 22:195–208
- Çağatay MN, Algan O, Sakıncı M, Eastoe C, Egesel L, Balkis N, Ongan D, Caner H (1999) A late Holocene sapropelic sediment unit from the southern Marmara shelf and its palaeoceanographic significance. *Quat Geol Rev* 18:531–540
- Çağatay MN, Kuşçu İ, Okay Aİ (2000a) Marmara Sea: morphology and structural geology. In: Meteor Berichte 00-3, Cruise no 44, 22 January–16 May 1999. Fachbereich Geowissenschaften, Universität Bremen, pp 33–36
- Çağatay MN, Görür N, Algan O, Eastoe C, Tchepalyga A, Ongan D, Kuhn T, Kuşçu İ (2000b) Late glacial holocene palaeoceanography of the Sea of Marmara: timing of connections with the Mediterranean and the Black Seas. *Mar Geol* 167:191–206
- Çağatay MN, Görür N, Polonia A, Demirbağ E, Sakıncı M, Cormier M-H, Capotondi L, McHugh L, Emre C, Eriş K (2003) Sea level changes and depositional environments in the İzmit Gulf, eastern Marmara Sea, during the late glacial-Holocene period. *Mar Geol* 202:159–173
- Carton H, Singh SC, Him A, Bazin S, de Voogd B, Vigner A, Ricolleau A, Cetin S, Ocakoglu N, Karakoc F, Sevilgen V (2007) Seismic imaging of the three-dimensional architecture of the Çınarcık Basin along the North Anatolian Fault. *J Geophys Res* 112:B06101. doi:10.1029/2006JB004548
- Cita MB, Aloisi G (2000) Deep-sea tsunami deposits triggered by the explosion of Santorini (3500 a BP), Eastern Mediterranean. *Sed Geol* 135:181–203
- Cita MB, Rimoldi B (1997) Geological and geophysical evidence for a Holocene tsunami deposit in the Eastern Mediterranean deep-sea record. *J Geodynamics* 24(1/4):293–304
- Demirbağ E, Rangin C, Le Pichon X, Şengör MC (2003) Investigation of the tectonics of the main Marmara fault by means of deep-towed seismic data. *Tectonophysics* 361:1–19
- Eriş K (2007) Middle Pleistocene to recent sea level changes in the Sea of Marmara (in Turkish with English abstract). PhD Thesis, Eurasia Institute of Earth Sciences, Istanbul Technical University
- Fine IV, Rabinovich AB, Thomson RE, Kulikov EA (2003) Numerical modeling of tsunami generation by submarine and subaerial landslides. In: Yalçınar AC, Pelinovsky E, Synolakis C, Okal E (eds) Submarine landslides and tsunamis. Proc NATO advanced research workshop underwater ground failures on tsunami generation, modeling, risk and mitigation, Istanbul. NATO science series, vol 21. Kluwer, Dordrecht, pp 69–88
- Gaudette H, Flight W, Tones L, Folger D (1974) An inexpensive titration method for the determination of organic carbon in recent sediments. *J Sediment Petrol* 44:249–253
- Gazioğlu C, Gökaşan E, Algan O, Yücel Z, Tok B, Doğan E (2002) Morphologic features of the Marmara Sea from multi-beam data. *Mar Geol* 190:397–420
- Gazioğlu C, Yücel ZY, Doğan E (2005) Morphological features of major submarine landslides of Marmara Sea using multibeam data. *J Coast Res* 21:664–673
- Geist EL (2000) Origin of the 17 July, 1998 Papua New Guinea tsunami: earthquake or landslide? *Seismol Res Lett* 71:344–351
- Géli L, Henry P, Zitter T, Dupré S, Tryon M, Çağatay MN, Mercier de Lépinay B, Le Pichon X, Şengör AMC, Görür N, Natalin B, Uçarkus G, Özeren S, Volker D, Gasperini L, Burnard P, Bourlange S, Party MS (2008) Gas emissions and active tectonics within the submerged section of the North Anatolian Fault zone in the Sea of Marmara. *Earth Planet Sci Lett* 274(1/2):34–39
- Gökaşan E, Gazioğlu C, Alpar B, Yücel ZY, Ersoy S, Gündoğdu O, Yaltrak C, Tok B (2002) Evidence of NW extension of the North Anatolian Fault Zone in the Marmara Sea: a new interpretation of the Marmara Sea (Izmit) earthquake on 17 August 1999. *Geo-Mar Lett* 21:183–199. doi:10.1007/s00367-001-0088-0
- Gökaşan E, Ustaömer T, Gazioğlu C, Yücel ZY, Öztürk K, Tur H, Ecevitoglu B, Tok B (2003) Morpho-tectonic evolution of the Marmara Sea inferred from multi-beam bathymetric and seismic data. *Geo-Mar Lett* 23:19–33. doi:10.1007/s00367-003-0120-7
- Gökçeoğlu C, Tunusluoğlu MC, Gorum T, Tur H, Gökaşan E, Tekkeli AB, Batuk F, Alp H (2009) Description of dynamics of the Tuzla landslide and its implications for further landslides in the northern slope and shelf of the Çınarcık Basin (Marmara Sea, Turkey). *Eng Geol* 106:133–153
- Görür N, Çağatay N, Sakıncı M, Sumengen M, Şentürk K, Yaltrak C, Tchepalyga A (1997) Origin of the Sea of Marmara as deduced from Neogene to Quaternary paleogeographic evolution of its frame. *Int Geol Rev* 39:342–352
- Grilli ST, Horillo J (1997) Numerical generation and absorption of fully nonlinear periodic waves. *J Eng Mech* 123(10):1060–1069
- Grilli ST, Watts P (1999) Modeling of waves generated by a moving submerged body: applications to underwater landslides. *Eng Anal Bound Elem* 23(8):645–656
- Grilli ST, Vogelmann PS, Watts P (2002) Development of a 3D numerical wave tank for modeling tsunami generation by underwater landslides. *Eng Anal Bound Elem* 26:301–313

- Hampton MA, Locat J (1996) Submarine landslides. *Rev Geophys* 34:33–59
- Harbitz CB (1992) Model simulations of tsunamis generated by the Storegga slides. *Mar Geol* 105:1–21
- Harbitz C, Pedersen G, Gjevik B (1993) Numerical simulations of large water waves due to landslides. *J Hydraul Eng* 119 (12):1325–1342
- Hayir A, Seseogullari B, Kilinc İ, Erturk A, Cigizoglu HK, Kabdasli MS, Yagci O, Day K (2008) Scenarios of tsunami amplitudes in the north eastern coast of Sea of Marmara generated by submarine mass failure. *Coast Eng* 55(5):333–356
- Hébert H, Piatanesi A, Heinrich F, Schindelé F, Okal EA (2002) Numerical modeling of the September 13, 1999 landslide and tsunami on Fatu Hiva Island (French Polynesia). *Geophys Res Lett* 29(10):1484. doi:10.1029/2001GL013774
- Hébert H, Schindelé F, Altinok Y, Alpar B, Gazioglu C (2005) Tsunami hazard in the Marmara Sea (Turkey): a numerical approach to discuss active faulting and impact on the İstanbul coastal areas. *Mar Geol* 215:23–43
- Imran J, Harff P, Parker G (2001) A numerical model of submarine debris-flow with graphical user interface. *Computer Geosci* 27:717–729
- İmren C, Le Pichon X, Rangin C, Demirbağ E, Ecevitoglu B, Görür N (2001) The North Anatolian Fault within the Sea of Marmara: a new interpretation based on multi-channel seismic and multi-beam bathymetry data. *Earth Planet Sci Lett* 186:143–158
- Kaminski MA, Aksu A, Box M, Hiscott RN, Filipescu S, Al-Salameen M (2002) Late Glacial to Holocene benthic foraminifera in the Marmara Sea: implications for Black Sea–Mediterranean Sea connections following the last deglaciation. *Mar Geol* 190:165–202
- Keller J, Ryan F, Ninkovitch D, Altherr R (1978) Explosive volcanic activity in the Mediterranean over the past 200, 000 yr recorded in deep sea sediments. *Geol Soc Am Bull* 89:591–604
- Ketin I (1953) Tektonische Untersuchungen auf den Prinzeninseln nahe İstanbul (Türkei). *Geol Rundsch* 41(1):161–172
- Ketin I, Guner G (1988) Structural peculiarity of the Carboniferous Thracian formation in the İstanbul area. *Muhendislik Jeolojisi Bulteni* 11:13–18
- Kilinc İ, Hayir A, Cigizoglu HK (2009) Wave dispersion study for tsunami propagation in the Sea of Marmara. *Coast Eng* 56:982–991
- Le Pichon X, Şengör AMC, Demirbağ E, Rangin C, İmren C, Armijo R, Görür N, Çağatay N, Mercier de Lépinay B, Meyer B, Saatçiler R, Tok B (2001) The active main Marmara fault. *Earth Planet Sci Lett* 192:595–616
- Liu PLF, Wu TR, Raichlen F, Synolakis CE, Borrero JC (2005) Runup and rundown generated by three-dimensional sliding masses. *J Fluid Mech* 536:107–144
- Loring DH, Rantala RTT (1992) Manual for the geochemical analyses of marine sediments and suspended particulate matter. *Earth-Sci Rev* 32:235–283
- Masson DG, Harbitz CB, Wynn RB, Pedersen G, Loholff F (2006) Submarine landslides: processes, triggers and hazard prediction. *Philos Trans R Soc Math Phys Eng Sci* 364:2009–2039
- McHugh CMG, Seeber L, Cormier M-H, Dutton J, Çağatay N, Polonia A, Ryan WBF, Görür N (2006) Submarine earthquake geology along the North Anatolia Fault in the Marmara Sea, Turkey: a model for transform basin sedimentation. *Earth Planet Sci Lett* 248:661–684
- McKenzie DP (1972) Active tectonics of Mediterranean region. *Geophys J R Astron Soc* 30:109–185
- Nyst M, Thatcher W (2004) New constraints on the active tectonic deformation of the Aegean. *J Geophys Res* 109:B11406. doi:10.1029/2003JB002830
- Okal EA, Synolakis CE (2001) Comment on ‘Origin of the 17 July 1998 Papua New Guinea tsunami: earthquake or landslide?’ by E.L. Geist. *Seismol Res Lett* 72(3):363–366
- Okay AI, Kaşlılar ÖA, İmren C, Boztepe GA, Demirbağ E, Kuşçu İ (2000) Active faults and evolving strike-slip basins in the Marmara Sea, northwest Turkey: a multichannel seismic reflection study. *Tectonophysics* 321:189–218
- Örgülü G, Aktar M (2001) Regional moment tensor inversion for strong aftershocks of the August 17, 1999 Izmit earthquake (Mw=7.4). *Geophys Res Lett* 28:371–374
- Özeren MS (2002) Crustal structure and forces in continental deformation. PhD Thesis, University of Cambridge, Cambridge
- Özeren MS, Postacioglu N, Zora B (2007) A new spectral algorithm for 3-D wave field in deep water. In: Inan E, Kiris A (eds) *Vibration problems ICOVP 2005*. Springer Proceedings in Physics, vol 111. Springer, Heidelberg, pp 395–402
- Pareschi MT, Boschi E, Favalli M (2006) Lost tsunamis. *Geophys Res Lett* 33:L22608. doi:10.1029/2006GL027790
- Pareschi MT, Boschi E, Favalli M (2007) Holocene tsunamis from Mount Etna and the fate of Israeli Neolithic communities. *Geophys Res Lett* 34:L16317. doi:10.1029/2007GL030717
- Parke JR, Minshull TA, Anderson G, White RS, McKenzie DP, Kucsu I, Bull JM, Görür N, Şengör AMC (1999) Active faults in the Sea of Marmara, western Turkey, imaged by seismic reflection profiles. *Terra Nova* 11(5):223–227
- Parke JR, White RS, McKenzie D, Minshull TA, Bull JM, Kuşçu I, Görür N, Şengör C (2002) Interaction between faulting and sedimentation in the Sea of Marmara, western Turkey. *J Geophys Res* 107(B11), 2286. doi:10.1029/2001JB000450
- Pelinovsky E, Poplavsky A (1996) Simplified model of tsunami generation by submarine landslides. *Phys Chem Earth* 21 (1/2):13–17
- Polonia A, Gasperini L, Amorosi A, Bonatti E, Çağatay N, Capotondi L, Cormier MH, Görür N, McHugh C, Seeber L (2004) Holocene slip rate of the North Anatolian Fault beneath the Sea of Marmara. *Earth Planet Sci Lett* 227:411–426
- Postacioglu N, Özeren MS (2008) A semi-spectral approach to landslide tsunamis. *Geophys J Int* 175(2):1–16
- Sarı E, Çağatay MN (2006) Turbidities and their association with past earthquakes in the deep Çınarcık Basin of the Marmara Sea. *Geo-Mar Lett* 26:69–76. doi:10.1007/s00367-006-0017-3
- Şengör AMC (1979) The North Anatolian transform fault; its age, offset and tectonic significance. *J Geol Soc Lond* 136:269–282
- Şengör AMC, Özgül N (2009) The climate and geology of İstanbul (in Turkish). In: *Encyclopaedia of İstanbul*, NTV Press, İstanbul (in press)
- Şengör AMC, Görür N, Şaroğlu F (1985) Strike-slip faulting and related basin formation in zones of tectonic escape: Turkey as a case study. In: Biddle KT, Christie Blich N (eds) *Strike-slip deformation, basin formation, and sedimentation*. *Soc Econ Paleontol Mineral Spec Publ* 37:228–264
- Şengör AMC, Tüysüz O, İmren C, Sakınç M, Eyidoğan H, Görür N, Le Pichon X, Rangin C (2004) The North Anatolian Fault. A new look. *Annu Rev Earth Planet Sci* 33:1–75
- Shanmugam G (2006) Deep-water processes and facies models: implications for sandstone petroleum reservoirs. *Handbook of petroleum exploration and production*, vol 5. Elsevier, Amsterdam
- Siyako M, Tanış T, Şaroğlu F (2000) Active fault geometry of the Sea of Marmara (in Turkish). *TUBITAK Bilim Teknik* 388:66–71
- Smith AD, Taymaz T, Oktay FY, Yüce H, Alpar B, Başaran H, Jackson JA, Kara S, Şimşek M (1995) High-resolution seismic profiling in the Sea of Marmara (northwest Turkey): Late Quaternary sedimentation and sea-level changes. *Bull Geol Soc Am* 107(8):923–936

- Soysal H, Sipahioğlu S, Kolçak D, Altinok Y (1981) A catalogue of earthquakes for Turkey and surrounding area (BC 2100–AD 1900). Final report, project number Tbag 341, Scientific and Technical Research Council of Turkey (TUBİTAK), Ankara
- Tappin DR, Watts P, McMurtry GM, Lafortune Y, Matsumoto T (2001) The Sissano, Papua New Guinea tsunami of July 1998—offshore evidence on the source mechanism. *Mar Geol* 175:1–23
- Tinti S, Armigliato A, Manucci A, Pagnoni G, Zaniboni F, Yalçiner AC, Altinok Y (2006a) The generating mechanisms of the August 17, 1999 İzmit Bay (Turkey) tsunami: regional (tectonic) and local (mass instabilities) causes. *Mar Geol* 225:311–330
- Tinti S, Pagnoni G, Zaniboni F (2006b) The landslides and tsunamis of 30th December 2002 in Stromboli analysed through numerical simulations. *Bull Volcanol* 68:462–479
- Tolun L, Çağatay MN, Carrigan WJ (2002) Organic geochemistry and origin of late glacial-Holocene sapropelic layers and associated sediments in Marmara Sea. *Mar Geol* 190:47–60
- Tur H (2007) An example of secondary fault activity along the north Anatolian Fault on the NE Marmara Sea Shelf, NW Turkey. *Earth Planets Space* 59:541–552
- Ustaömer T, Gökaşan E, Tur H, Görüm T, Batuk FG, Kalafat D, Alp H, Ecevitoglu B, Birkan H (2008) Faulting, mass-wasting and deposition in an active dextral shear zone, the Gulf of Saros and the NE Aegean Sea, NW Turkey. *Geo-Mar Lett* 28:171–193. doi:10.1007/s00367-007-0099-6
- Utkucu M, Kanbur Z, Alptekin Ö, Sünbül F (2009) Seismic behaviour of the North Anatolian Fault beneath the Sea of Marmara (NW Turkey): implications for earthquake recurrence times and future seismic hazard. *Nat Hazards* 50:45–71. doi:10.1007/s11069-008-9317-4
- Ward SN (2001) Landslide tsunami. *J Geophys Res* 106:11,201–11,215
- Watts P (1998) Wavemaker curves for tsunamis generated by underwater landslides. *ASCE J Waterw Port Coast Ocean Eng* 124(3):127–137
- Watts P (2000) Tsunami features of solid block underwater landslides. *ASCE J Waterw Port Coast Ocean Eng* 126(3):144–152
- Watts ST, Grilli JT, Kirby GJ, Fryer GJ, Tappin DR (2003) Landslide tsunami case studies using a Boussinesq model and a fully nonlinear tsunami generation model. *Nat Hazards Earth Syst Sci* 3:391–402
- Wulf S, Kraml M, Kuhn T, Schwarz M, Inthorn M, Keller J, Kuscü I, Halbach P (2002) Marine tephra from the Cape Riva eruption (22 ka) of Santorini in the Sea of Marmara. *Mar Geol* 183(1/4):131–141
- Yalçiner AC, Pelinovsky EN (2007) A short cut numerical method for determination of periods of free oscillations for basins with irregular geometry and bathymetry. *Ocean Eng* 34:747–757
- Yalçiner AC, Altinok Y, Synolakis CE (2000) Tsunami waves in İzmit Bay after the Kocaeli earthquake. In: *Earthquake Spectra Reconnaissance Report*, EERI, Oakland, CA, suppl vol 16, chap 3, pp 55–62
- Yalçiner AC, Alpar B, Altinok Y, Özbay I, Imamura F (2002) Tsunamis in the Sea of Marmara: historical documents for the past, models for the future. *Mar Geol* 190:445–463
- Yılmaz Y, Gökaşan E, Erbay AY (2009) Morphotectonic development of the Marmara region. *Tectonophysics* (in press). doi:10.1016/j.tecto.2009.05.012
- Zitter TAC, Henry P, Aloisi G, Delaygue G, Çağatay MN, Mercier de Lepinay B, Al-Samir MF, Fornacciari F, Tesmer M, Pekdeger A, Wallmann K, Lericolais G (2008) Cold seeps along the main Marmara Fault in the Sea of Marmara (Turkey). *Deep-Sea Res* 55:552–570